IEEE Access
Multidisciplinary | Rapid Review | Open Access Journal

IEEE POWER & ENERGY SOCIETY SECTION

Received February 26, 2021, accepted March 5, 2021, date of publication March 10, 2021, date of current version March 30, 2021.

Digital Object Identifier 10.1109/ACCESS.2021.3064888

Study on the Optimal Configuration of a Wind-Solar-Battery-Fuel Cell System Based on a Regional Power Supply

ZEKUN WANG[1,2,3], YAN JIA[1,4,5], CHANG CAI[2,3], YINPENG CHEN[1], NA LI[1], MIAO YANG[1], AND QING'AN LI[1,2,3]

[1]School of Energy and Power Engineering, Inner Mongolia University of Technology, Hohhot 010051, China
[2]Institute of Engineering Thermophysics, Chinese Academy of Sciences, Beijing 100190, China
[3]Key Laboratory of Wind Energy Utilization, Chinese Academy of Sciences, Beijing 100190, China
[4]Key Laboratory of Wind Energy and Solar Energy Utilization Technology, Ministry of Education, Inner Mongolia University of Technology, Hohhot 010051, China
[5]Inner Mongolia Autonomous Region Wind Power Technology and Testing Engineering Technology Research Center, Inner Mongolia University of Technology, Hohhot 010051, China

Corresponding authors: Yan Jia (2497331641@qq.com) and Chang Cai (caichang@iet.cn)

This work was supported in part by the Inner Mongolia Science and Technology Program under Grant 201601064, and in part by the Inner Mongolia Autonomous Region Science and Technology Major Special Project-Autonomous Region Engineering Technology Research Center Construction Project.

ABSTRACT The integration of energy storage facilities into existing structures will result in increased costs. Therefore, it is of great significance to optimize the configuration of integrated power systems with multienergy flows to reduce the cost of the comprehensive utilization of energy. This study established a wind-solar-battery-fuel cell integrated power supply system to optimize the grid-connected regional power supply. First, the load is given with a known daily energy demand. The optimization goal is to minimize the average annual cost and the loss of power supply probability. The cost model includes the constraints of transportation costs and the benefits of selling hydrogen and oxygen. Then, an improved genetic algorithm is developed to optimize the structure of the wind-solar-battery-fuel cell integrated power supply system. The basic idea of the improved genetic algorithm is to change the coordination mode of the crossover operator and the mutation operator according to the size of the initial population fitness. Finally, according to the calculation results of the improved genetic algorithm, the optimal configuration of the capacity of devices in the system is obtained, verifying the effectiveness of the improved genetic algorithm. The cost calculation result of the genetic algorithm is 18.7% higher than that of the improved genetic algorithm, and it completely converges at approximately 70 steps. The cost calculation result of the particle swarm optimization is 17.1% higher than that of the improved genetic algorithm, and it completely converges at approximately 75 steps. The cost calculation result of the nondominated sorting genetic algorithm is 9.6% higher than that of the improved genetic algorithm, and it completely converges at approximately 58 steps. The system established in this research can fully meet the power demands for a given area and effectively reduce the local curtailment of wind energy and solar energy.

INDEX TERMS Multienergy flow integrated power supply system, optimum ratio, improved genetic algorithm, average annual cost, loss of power supply probability.

I. INTRODUCTION

With the rapid growth of the global economy and population, energy demand is becoming increasingly. At present, the power supply is mainly based on fossil fuels such as coal and oil [1], [2]. However, harmful gases emitted by fossil fuels seriously affect human life, it is urgent to vigorously develop non-hydroelectric renewable energy [3]. The highly efficient and clean power-generating technology of renewable energy has been highly valued and applied worldwide [4]. Many clean energy sources, such as solar energy, wind energy and biomass energy, have been gradually utilized by people, and solar energy and wind energy are the most rapidly developing energy sources [5], [6]. However, wind and solar power generation are highly uncontrollable, so it is necessary for energy storage systems to ameliorate power

The associate editor coordinating the review of this manuscript and approving it for publication was Suman Maiti.

This work is licensed under a Creative Commons Attribution 4.0 License. For more information, see https://creativecommons.org/licenses/by/4.0/

fluctuations [7]. As a new energy storage method, hydrogen, combined with wind power and solar power, will greatly reduce the impacts on the power grid caused by unstable power supplies [8]. Electrolytic cells can efficiently utilize the excess power generated by wind and solar power generation to improve the power quality of the grid [9]. When power generation is insufficient to meet the electricity load, the fuel cell [10] compensates the power output. The energy density of hydrogen is large, which is convenient for transportation and storage. The use of hydrogen storage is an inevitable trend of future energy storage development [11]–[13]. Wind and solar power generation with the use of hydrogen storage to supplement the grid is more economical and feasible than adjusting the power imbalance of the grid itself. At present, wind-solar-fuel cell systems have been built in countries around the world. For example, in 2016, a joint wind-hydrogen energy office building system was successfully constructed in Scotland. The main components of the system are a wind turbine, alkaline electrolyzer, hydrogen storage and a PEM fuel cell. Unfortunately, this application did not include solar energy [14]. In 2020, the wind-solar hybrid power supply system was successfully constructed in Hubei Province, China. The booster station converts the voltage into 110 kV and sends it to the main grid. However, this system does not incorporate hydrogen fuel cells. Therefore, it is necessary to build a wind-solar-battery-fuel cell system. After the system is established, the top priority is to optimize the configuration of the system to reduce costs.

At present, for system optimization problems, optimization software and traditional optimization algorithms have been widely used. These software include the Matrix Laboratory (MATLAB) and Hybrid Optimization Model for Electric Renewables (HOMER). The traditional algorithms include the genetic algorithm (GA), particle swarm optimization (PSO), ant colony optimization (ACO) and so on. In Vaiju *et al.* [15], the authors presented a joint optimal allocation methodology of renewable distributed generation (RDG) and energy storage to achieve economic benefits and used a highly competitive algorithm called the grey wolf optimizer in MATLAB. They also used this method in Ref. [16], but the studies differed in that the goal of the latter was to minimize the energy loss. Li *et al.* [17] modeled and optimized different combinations of photovoltaic panels, wind turbines and biogas generators in HOMER. Kasprzyk *et al.* [18] used GA to optimize the structure of a hybrid off-grid power distribution system (with electrochemical energy storage). Similarly, Mayer *et al.* [19] used GA to optimize a multiobjective design framework for household-scale systems, which resulted in the lowest cost and the smallest environmental footprint options in a case study of three different locations across Europe. Other traditional algorithms have also been used. In Ref. [20], Javed *et al.* developed a mathematical model to optimize a hybrid solar-wind energy system with storage for a remote island with a genetic algorithm. Regarding other traditional algorithms, Guo *et al.* [21] proposed a wind-solar-thermal energy storage hybrid power system with an electric heater, and the capacity optimization was solved by a multiobjective PSO algorithm. Fetanat *et al.* [22] used ACO in their study of three renewable energy systems.

However, the traditional algorithms have some shortcomings in this kind of logical system optimization problem. For example, the traditional standard GA uses fixed control parameters [23], [24], which results in poor global searching ability. Otherwise, when the individual fitness gap is very small, the first crossover operation will increase the running time of the algorithm, and this will not make the result more accurate.

Others have used improved traditional algorithms for system optimization. Mohamed *et al.* [25] used the multiobjective water cycle algorithm to maximize environmental, technical, and economic benefits. In Ref. [26], Dong *et al.* presented an improved ACO algorithm for sizing a stand-alone hybrid solar-wind turbine-battery-hydrogen system, and they showed the effectiveness of the improved ACO algorithm through simulation experiments. Some scholars have also used an improved traditional genetic algorithm. Zhang *et al.* [27] applied the nondominated sorting genetic algorithm (NSGA-II) to analyze decision variables regarding the optimal numbers of wind turbines, solar modules and battery banks, with the total system cost (TSC) and the loss of power supply probability (LPSP) as the objective functions. In recent years, some scholars have improved NSGA-II. Xu *et al.* [28] used a modified NSGA-II based on reinforcement learning to determine a set of Pareto solutions. These new algorithms show good adaptability when optimizing the systems proposed in the corresponding studies. At present, many new algorithms have been proposed. However, there are few algorithms with the potential to be applied to the system we have proposed.

Therefore, we built the system by writing programs and developing the traditional GA. This paper uses an improved genetic algorithm (IGA) to optimize the wind-solar-battery-fuel cell multienergy flow integrated power supply system configuration to ensure that the load power shortage rate is zero while at the same time reducing the transportation cost and average cost and providing a configuration scheme for a regional power supply, proving the adaptability and effectiveness of the proposed algorithm, which can be used as a reference for future values. The concrete measure of this change to the algorithm is to improve the cooperation between the crossover operator and mutation operator. This improvement can make the algorithm jump out of the local optimal solution and allow the choice of whether to perform a crossover operation or mutation operation first according to the size of the individual fitness gap. This system can fully meet the power demand for a given area and effectively reduce the local curtailment of wind energy and solar energy.

The main contributions of this paper are summarized as follows.

1) In order to optimize the grid-connected regional power supply, a wind-solar-battery-fuel cell integrated power supply system is established. This system can fully meet

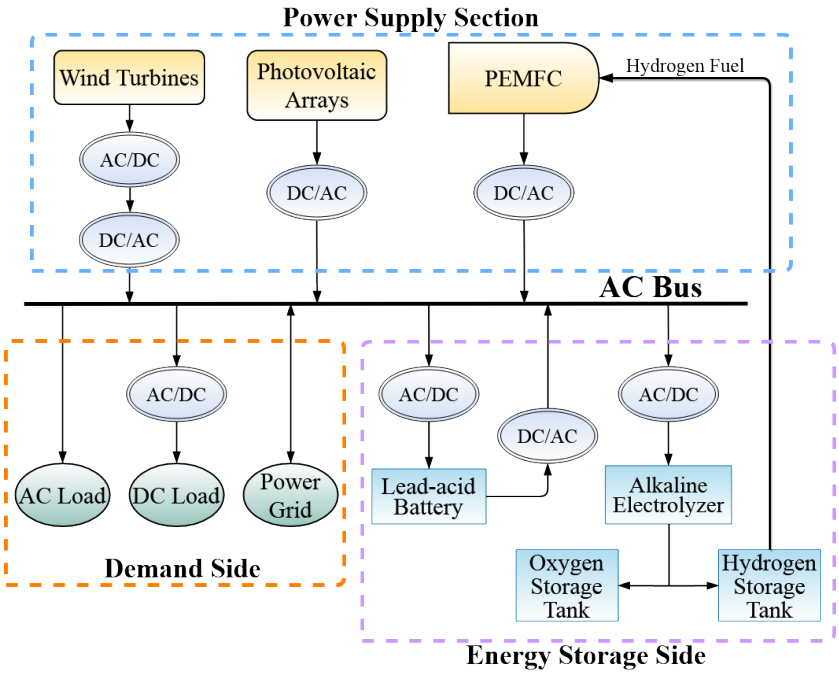

FIGURE 1. Structure diagram of a common AC bus system.

the power demand for a given area and effectively reduce the local curtailment of wind energy and solar energy caused by poor power generation due to equipment capacity configurations.

2) Considering the shortcomings of traditional genetic algorithms, we proposed an improved genetic algorithm to optimize the structure of the wind-solar-battery-fuel cell integrated power supply system. The results showed that improved genetic algorithm is superior to the other three algorithms in terms of optimization results and calculation speed. Verifies the good adaptability and effectiveness of the algorithm in strong logical multiobjective optimization problems
3) Although we have ignored some factors in this work, such as unstable output power, real-time changing load, etc. This does not affect the correctness of the optimization results. When building and applying the system in the future, this article can give a certain reference value.

This study is organized as follows. Section 2 introduces the structure of the wind-solar-battery-fuel cell multienergy flow integrated power supply system and the mathematical model of the main equipment in the system. Section 3 introduces the IGA enhancements and some of the code changes. Section 4 introduces the optimization objectives and constraints. In the fifth section, a numerical example is simulated and verified. Section 6 summarizes the conclusion.

II. SYSTEM STRUCTURE AND MATHEMATICAL MODEL OF THE SYSTEM

In this section, we introduce the structure and operational mode of a wind-solar-battery-fuel cell multienergy flow integrated power supply system in detail. The equivalent mathematical model of each piece of equipment is established in turn, including the wind turbine, photovoltaic array, lead-acid battery, alkaline electrolyzer and proton exchange membrane fuel cells (PEMFCs).

A. SYSTEM STRUCTURE AND OPERATIONAL MODE

In this paper, the proposed wind-solar-battery-fuel cell multienergy flow integrated power supply system consists of a wind turbine, photovoltaic array, lead-acid battery, alkaline electrolyzer, PEMFC and its components, inverter, rectifier and other parts. The system has two operating modes to choose from: a common DC bus structure or a common AC bus structure [29], [30]. An AC bus system is applied in this paper, and its structure is shown in FIGURE 1. (The arrows in FIGURE 1 represents the direction of energy flow).

FIGURE 2 shows that the system has two complementary operational modes based on the comparison of the input power and load demand: when the input power is greater than the load demand, the excess power successfully meets the maximum capacity of the battery and the maximum capacity of the hydrogen storage tank. If there is still a power surplus, it is sold to the grid. When the input power is less than the load demand, the power shortage is replenished by the battery. If the battery has been discharged to its minimum, then hydrogen fuel enters the PEMFC to continue to supply the load. If the power demand still cannot be met, the system purchases power from the grid to meet the load.

B. WIND TURBINE

The output power of a wind turbine is closely related to the wind speed, blade inclination, and blade material. In this paper, wind speed is only considered as a single variable, and

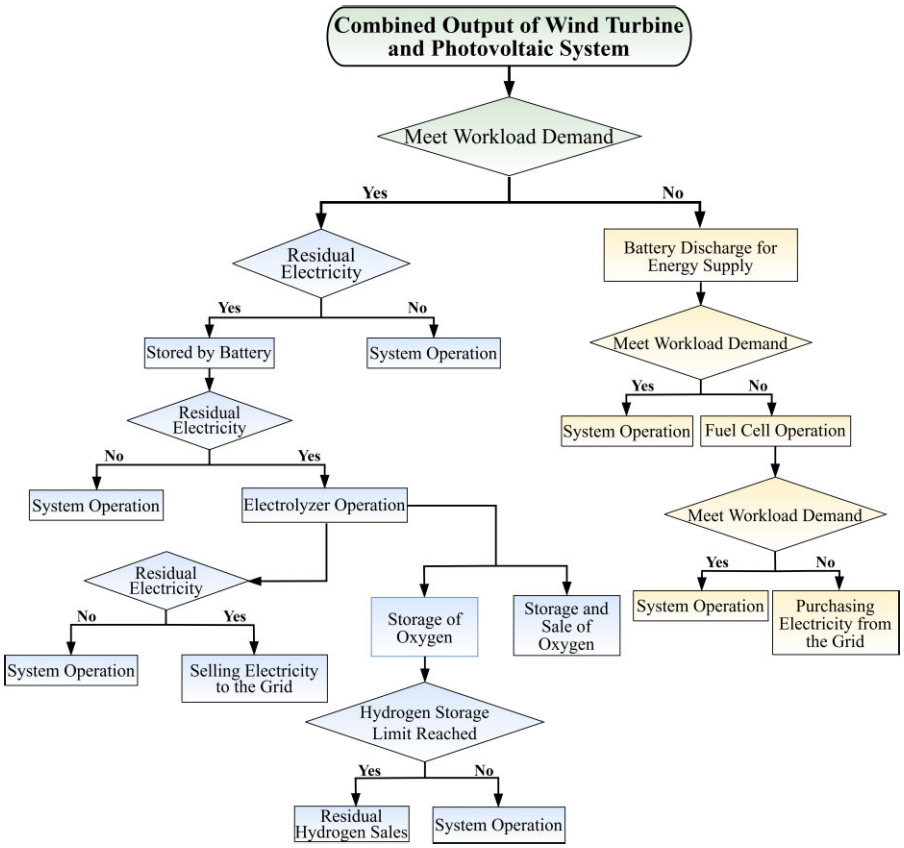

FIGURE 2. Flow chart of the operational modes of the system.

the equivalent mathematical model is shown as follows [15].

$$P_W(t) = \begin{cases} 0 & v(t) < v_{ti},\ v(t) > v_{to} \\ nA\left[v(t)\right]^3 - nBP_N & v_{ti} \le v(t) \le v_N \\ nP_N & v_N \le v(t) \le v_{to} \end{cases} \quad (1)$$

In the formula: $P_W(t)-$ the output power of the wind generator at time t; $v(t)-$ the wind speed at the rotating shaft of the wind turbine at time t; $v_{ti}-$ the cut-in wind speed of the wind turbine; $v_{to}-$ the cut-out wind speed of the wind turbine; v_n- the rated wind speed of the wind turbine; $n-$ the number of wind turbines operating in the system; P_N- the rated power of each wind turbine per unit number; and coefficients A and B are determined by the following formulas: $A = nP_N/\left(v_N^3 - v_{ti}^3\right) B = v_{ti}^3/\left(v_N^3 - v_{ti}^3\right)$.

C. PHOTOVOLTAIC ARRAY

The principle of photovoltaic arrays current generation is based on the solar effect generated by a semiconductor. The equivalent mathematical model of its output power is shown as follows [31].

$$P_{PV} = P_{stc}G_w\frac{\left[1 + K\left(T_w - T_0\right)\right]}{G_{stc}} \quad (2)$$

In the formula: $P_{PV}-$ the output power of the photovoltaic array; $P_{stc}-$ the maximum solar output power under standard test conditions; G_w- the light intensity of the photovoltaic array at work; $K-$ the power temperature coefficient; T_w- the temperature at the photovoltaic array operation; T_0- the temperature of the test environment; and $G_{stc}-$ the light intensity under standard test conditions.

D. LEAD-ACID BATTERY

The voltage, temperature and electrolyte concentration of a lead-acid battery affect the battery charging and discharging processes. This paper assumes that the voltage is constant and that the temperature is controlled within an appropriate range. The equivalent mathematical model is as follows [32], taking into account the remaining quantity of electricity in the battery and the charging and discharging efficiency.

Case 1: Battery charging

$$\begin{cases} \left[W_f(t) + W_{PV}(t)\right] \times \eta_{inv} - E_l(t) > 0 \\ S_C(t-1) < S_{C\max} \end{cases} \quad (3)$$

$$S_C(t) = (1-\delta)S_C(t-1) + \left(P_C\Delta t\eta_C\right)/E_C \quad (4)$$

Case 2: Battery discharging

$$\begin{cases} \left[W_f(t) + W_{PV}(t)\right] \times \eta_{inv} - E_l(t) < 0 \\ S_C(t-1) > S_{C\min} \end{cases} \quad (5)$$

$$S_C(t) = (1-\delta)S_C(t-1) - \left(P_D\Delta t\right)/E_C\eta_D \quad (6)$$

In the formulas above: $W_f(t)-$ the generating capacity of the wind turbine at time t; $W_{PV}(t)-$ the power generation

of the photovoltaic panels at time t; η_{inv}, η_C, η_D the inverter efficiency and battery charging and discharging efficiencies, respectively; $E_l(t)$ the power consumption of the load at time t; $S_C(t)$, $S_C(t-1)$ – the electric quantity stored in the battery at time t and $(t-1)$; $S_{C\max}$, $S_{C\min}$ – the maximum and minimum amount of electricity that can be stored by the battery; δ – the self-discharge rate of the battery; P_C, P_D – the charging and discharging power of the battery, respectively; and E_C – the rated capacity of the battery.

E. ALKALINE ELECTROLYZER SYSTEM

An alkaline electrolyzer is composed of an alkaline electrolyte (KOH aqueous solution), a diaphragm, and a metallic anode and cathode. [33]. In this paper, it is assumed that the electrolytic cell is always operating at an appropriately high temperature. The mathematical models of the alkaline cell and its components are as follows [34].

$$P_{NE} = \frac{2Q_N \times N_A \times V_N}{3600 \times V_m \times C_0 \times \eta_E} \tag{7}$$

$$Q = \frac{P_{\mathrm{t}} \times Q_N}{P_{NE}} \tag{8}$$

Capacity of the alkaline electrolyzer:

$$N_E = \frac{\max P_{net}}{P_{NE}} \tag{9}$$

Capacity of the hydrogen storage tank:

$$N_{t1} = \frac{\max Q_{net}}{P_t} \tag{10}$$

$$Q_{net} = Q_t \times P_{NE}/C_N/r \tag{11}$$

The relationship between hydrogen storage and gas input is shown as follows.

$$N'_{t1} = Q_S \times \eta_T \tag{12}$$

Ignoring the fact that external conditions affect the yields of hydrogen and oxygen, this paper simplifies the production of hydrogen as two times that of oxygen, as follows.

$$Q_{H2} = 2 \times Q_{O2} \tag{13}$$

In the formulas above: Q_N – the hydrogen yield under ideal conditions; P_{NE} – the rated power of the alkaline electrolyzer; N_A – the Avogadro constant, 6.02×10^{23}; C_0 – the number of electrons per coulomb, 6.25×10^{18}; V_m – the molar volume of gas in the standard state, 24.5 *L/mol*; V_N – the output voltage; η_E – the conversion efficiency of the alkaline electrolyzer; Q – the volume of hydrogen gas; P_t – the equivalent power of a Q volume of hydrogen; N_E – the capacity of the alkaline electrolyzer; P_{net} – the net power of the wind-solar-battery-fuel cell multienergy flow integrated power supply system; N_{t1} – the capacity of the hydrogen storage tank; Q_{net} – the net energy accumulation of the wind-solar-battery-fuel cell multienergy flow integrated power supply system; Q_t – the equivalent chemical energy of a Q volume of hydrogen; C_N – the hydrogen storage tank capacity per unit; r – the hydrogen compression ratio; N'_{t1} – the actual hydrogen storage amount; Q_S – the amount of hydrogen gas input by the alkaline electrolyzer; η_T – the hydrogen storage efficiency; Q_{H2} – the actual hydrogen production; and Q_{O2} – the actual oxygen production.

F. THE PROTON EXCHANGE MEMBRANE FUEL CELL (PEMFC) SYSTEM

PEMFCs can supplement the battery when the lead-acid battery cannot meet the load demand.

The output power of the fuel cell can be regarded as the reverse process of the alkaline electrolyzer. The simplified mathematical model is as follows [35].

$$P_{NFC} = \frac{2N'_{t1} \times N_A \times V_N \times \eta_{FC}}{3600 \times V_m \times C_0} \tag{14}$$

The capacity of the PEMFC is determined by the following formula:

$$N_{FC} = |\min(P_{net})/P_{FC}| \tag{15}$$

In the formula: P_{NFC} – the output power of the PEMFC; η_{FC} – the conversion efficiency of the PEMFC; N_{FC} – the capacity of the PEMFC; P_{FC} – the energy supply power of the PEMFC.

III. IMPROVED GENETIC ALGORITHM

As mentioned in the introduction, the GA has large limitations. If the initial population diversity is poor and the individual fitness gap is small, the algorithm is more likely to fall into a local optimal solution and fail to reach the global optimal solution. Compared with other parameter optimization methods, genetic algorithm is more suitable to use binary representation to solve problems. However, traditional GA only effectively optimizes the objective function without limitation. The binding constraints interfere with the efficiency of the search process in GA. In addition, the existing GA has a problem that when the system is large in scale and when it runs in a wide search space including infeasible solutions, the calculation time is very long. The subsequent calculation results also illustrate this problem. When the PSO converges, all particles are close to the optimal solution, resulting in lower population diversity and lower accuracy. In view of the above shortcomings, we have made some improvements to the traditional GA. The GA crossover operator [36], [37] and mutation operator [36], [38]–[40] are improved to make the algorithm more accurate and less time-consuming. Therefore, a fitness judgment method was introduced involving a comparison between the arccosine of the ratio between the average individual fitness (F_1) divided by the maximum population fitness (F_2) and $\pi/3$.

When $(F_1/F_2) \geq \pi/3$, the gap between the average individual fitness and the largest fitness value is large, the system is species rich, and we try to reduce the superiority of the gene mutation probability to prevent damage by increasing the crossover probability of the evolution of individual qualities.

When $(F_1/F_2) \geq \pi/3$, at this point, the gap between the average individual fitness and the largest fitness value is

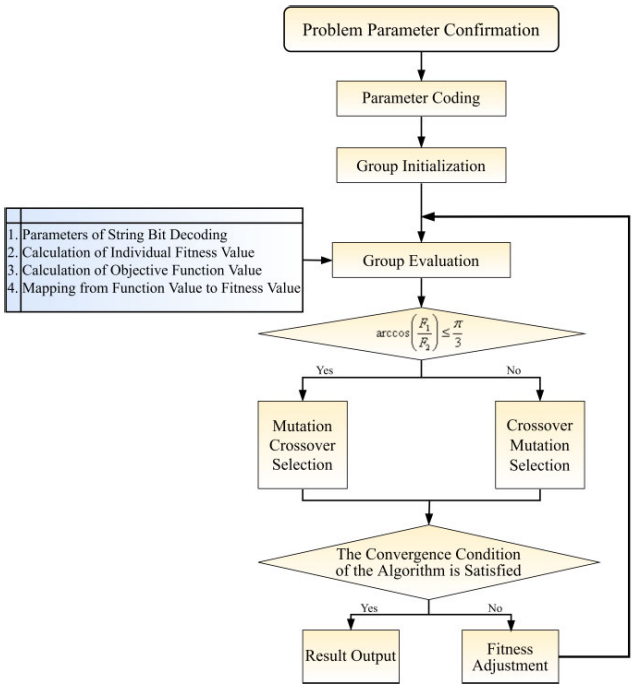

FIGURE 3. Flow chart of the IGA calculation.

small, and the crossover probability of individual qualities is very small, which should reduce the crossover probability to save running time and increase the mutation probability to search for the global optimal value.

The flow chart of the improved genetic algorithm is as follows.

When the optimal individual fitness reaches a certain target value, the optimal individual fitness and group fitness do not change or the number of iterations reaches a preset upper limit (100-500 generations), the algorithm will be terminated. In this paper, the IGA initial parameters were set as follows: number of individuals: 100, maximum genetic algebra: 120, variable binary digit: 8, generation gap: 0.25, crossover probability: 0.8, mutation probability: 0.01.

A small part of the improved code is as follows:

$$
\begin{aligned}
&k_1 = 1; \quad k_2 = 0.05; \; k_3 = 0.02; \; k_4 = 2; \\
&F_1 = mean\,(ObjV)\,; \quad F_2 = \max\,(ObjV)\,; \\
&if \;\; a\cos\,(F_1/F_2) \le pi/3 \\
&\quad cross - prob = k_1 \times (1 - a\cos\,(F_1/F_2)\,/\,(pi/2))\,; \\
&\quad vray - prob = k_2 \times a\cos\,(F_1/F_2)\,/\,(pi/2)\,; \\
&else \\
&\quad vray - prob = k_3 \times (1 - a\cos\,(F_1/F_2)\,/\,(pi/2))\,; \\
&\quad cross - prob = k_2 \times a\cos\,(F_1/F_2)\,/\,(pi/2)\,; \\
&end
\end{aligned} \tag{16}
$$

In the code above: $ObjV-$ the population fitness; $cross-prob-$ the crossover probability; $vray-prob-$ the variation probability; $a\cos-$ the inverse cosine function; and $pi-\pi$, approximately equal to 3.14.

IV. OPTIMIZATION MODEL OF A WIND-SOLAR-BATTERY-FUEL CELL MULTIENERGY FLOW INTEGRATED POWER SUPPLY SYSTEM

A. OPTIMIZATION GOAL

The premise of system optimization is to minimize the cost of a whole system while ensuring the normal operation of all loads [4]. In this paper, the full cycle cost of the system is converted into an annual mean cost for the analysis and calculations, and the function model is established as follows.

$$C_T = C_a + C_p - C_{H2} - C_{O2} - C_s \tag{17}$$

In the formula: C_T- the annual total cost of the wind-solar-battery-fuel cell multienergy flow integrated power supply system; C_a- the annual mean cost of the system equipment; C_p- the annual power purchase cost of the system; C_{H2}, $C_{O2}-$ the annual hydrogen and oxygen sales revenue of the system; and C_s- the annual electricity sales revenue of the system.

The detailed calculation method is as follows.

$$C_a = C_0 \times \frac{i\,(1+i)^n}{(1+i)^n - 1} \tag{18}$$

$$C_0 = C_w + C_w^{in} + C_{pv} + C_{pv}^{in} + C_{bat} + C_{bat}^{in} + C_E + C_E^{in} + C_{FC} + C_{FC}^{in} \tag{19}$$

$$C_p = S_p \times Q_p \tag{20}$$

$$C_{H2} = S_{H2} \times Q_{H2} \tag{21}$$

$$C_{O2} = S_{O2} \times Q_{O2} \tag{22}$$

$$C_s = S_s \times Q_s \tag{23}$$

In the formulas above: C_0- the full cycle cost of the wind-solar-battery-fuel cell multienergy flow integrated power supply system; $i-$ the discount rate; $n-$ the system life; C_w, C_{pv}, C_{bat}, C_E, $C_{FC}-$ the initial investments of the wind turbines, photovoltaic panels, lead-acid batteries, alkaline electrolyzers and PEMFCs, respectively; C_w^{in}, C_{pv}^{in}, C_{bat}^{in}, C_E^{in}, $C_{FC}^{in}-$ the full-cycle operation and maintenance costs of the wind turbines, photovoltaic panels, lead-acid batteries, alkaline electrolyzers and PEMFCs, respectively; S_p, S_s- the annual electricity purchase and sales of the system; Q_p, Q_s- the unit price of purchasing electricity and selling electricity; S_{H2}, $S_{O2}-$ the amount of hydrogen and oxygen produced by the system throughout the year; Q_{H2}, $Q_{O2}-$ the unit price of hydrogen and oxygen.

B. CONSTRAINTS IN THE WIND-SOLAR-BATTERY-FUEL CELL MULTIENERGY FLOW INTEGRATED POWER SUPPLY SYSTEM OPTIMIZATION

The optimal configuration of the system is based on the following constraints.

1) OUTPUT POWER OF EACH PIECE OF EQUIPMENT IN THE SYSTEM

The number of wind turbines, photovoltaic arrays and batteries shall be greater than zero:

$$Min\left(P_w, N_{pv}, N_{bat}\right) > 0 \tag{24}$$

In the formula: P_w – the output power of the wind turbines; and N_{pv}, N_{bat} – the number of photovoltaic panels and batteries, respectively.

2) SOC OF BATTERIES

At any time t, the charged state of the battery should be between the minimum and the maximum.

$$SOC_{\min} \leq SOC\ (t) \leq SOC_{\max} \tag{25}$$

In the formula: $SOC_{\min}$ – the minimum value of the remaining power of the battery; $SOC_{\max}$ – the maximum value of the remaining power of the battery; and $SOC\ (t)$ – the remaining electric quantity in the battery at the moment of time t.

3) LOSS OF POWER SUPPLY PROBABILITY (LPSP)

The LPSP is an index reflecting the power supply reliability of the system and is defined as the ratio of the system outage time and power supply time. When the input power of the system cannot meet the load demand, power is purchased from the grid, and the loss of power supply probability should be zero [41].

It is very important to consider the LPSP [42]–[44]. We must meet the load power demand; only in this way is our research meaningful. In other words, we must reduce the system cost on the basis of meeting the load demand.

Considering the energy accumulation of the storage battery, to accurately show the operation of the system, the time sequence method is used to characterize the LPSP. The mathematical model is as follows.

$$LPSP = \frac{\sum_{t=0}^{8760} TIME\ (P_{available}\ (t) < P_{needed}\ (t))}{T_t} = 0 \tag{26}$$

In the formula: $TIME\ (P_{available}\ (t) < P_{needed}\ (t))$ – the power shortage time, referring to the time when the power generation equipment generates insufficient power and the battery capacity reaches the minimum, and $TIME$ – time; $P_{available}\ (t)$ – the available electricity generated by wind turbines and solar panels according to the time; $P_{needed}\ (t)$ – the load demand power according to the time; and T_t – the total time of data input.

4) THE STATE OF HYDROGEN STORAGE IN THE SYSTEM

The hydrogen storage capacity shall not exceed the maximum capacity of the hydrogen storage tank.

$$N'_{t1} \leq N_{t1} \tag{27}$$

5) THE STATE OF OXYGEN STORAGE IN THE SYSTEM

The oxygen storage capacity shall not exceed the maximum capacity of the oxygen storage tank:

$$N'_{t2} \leq N_{t2} \tag{28}$$

In the formula: N'_{t2} – the actual oxygen storage volume and N_{t2} – the oxygen tank volume.

V. EXAMPLE SIMULATION

A. PARAMETERS OF THE MAIN EQUIPMENT

All the parameters of the equipment in this paper are obtained from the corresponding manufacturers, and the data are authentic.

The system includes a three-blade horizontal-axis wind turbine with a rated power of 8000 W, a photovoltaic panel with a peak power of 250 W, a 12 V-240Ah lead-acid battery, an alkaline electrolyzer with a rated power of 6000 W, and a PEMFC with a rated power of 5000 W. The economic parameters (transportation cost added into the wind turbine construction cost) of these equipment are as follows.

Parameters of the wind turbine.

Parameters of the lead-acid battery.

Parameters of the alkaline electrolyzer and PEMFC.

For the time-of-use electricity prices [45], this paper divides the 24 hours of the day into different time periods, and the electricity purchase and sale prices are different in each time period.

B. DATA SOURCES FOR THE EXAMPLE CALCULATION

The wind speed, irradiance and load demand data of a town in Erenhot, Xilin Gol League, Inner Mongolia Autonomous Region, China, in 2019 are selected as data sources, and the local wind speed in 2019 is shown as follows. The data were obtained from a wind farm in the study area.

FIGURE 4 shows the measured wind speed data in 2019 ranging from 4 m/s to 25 m/s. The wind speed data are sampled every 10 min, with a total of 52,560 sampling times in the whole year. The irradiance data are calculated using the annual hourly average.

The output power of a photovoltaic panel is affected by the working temperature and partial shading effect. However, through continuous monitoring of the working temperatures of photovoltaic panels and considering that the output power deviates from the working goal. Considering the partial shading effect will bring great difficulty to our work, and this factor will not greatly affect the conclusion of this article. We assumed that the working temperatures of photovoltaic panels are consistent with the rated temperatures and the output power of photovoltaic panels had no partial shading effect. The irradiance and ambient temperature have an impact on the output power. The irradiance data were obtained from a photovoltaic power station in the study area.

In the study area, the load of local users is closely related to the season. In fact, the demand for electricity is changing all the time. However, if we consider all the changes in electricity consumption, it will lead to a huge workload and not much significance. Therefore, we only consider the maximum power consumption in each period. The load curve is shown as follows. The data were obtained from a power supply bureau in the study area.

On the whole, the load in this area is higher in summer and winter and lower in spring and autumn; these trends are closely related to the local electricity demand.

TABLE 1. Economic parameters of each piece of equipment.

Equipment	Cost of construction/CNY	Operation and maintenance cost (20 years)/CNY	Replacement cost (20 years)/CNY	Service life /year
Wind turbine	66000	39600	0	20
Photovoltaic panel	1750	3500	0	20
Lead-acid battery	1440	2880	3900	5
Alkaline electrolyzer	38160	7200	0	20
PEMFC	15000	6900	42000	5

TABLE 2. Parameters of the wind turbine.

Rated power/W	Height of the tower/m	Cut-in wind speed/m · s^{-1}	Cut-out wind speed/m · s^{-1}	Rated wind speed/m · s^{-1}
8000	10	4	25	10

TABLE 3. Parameters of the lead-acid battery.

Nominal capacity/Ah	Rated voltage/V	Number of charges and discharges	Safe power range	Depth of discharge
240	12	6000	20-85%	85%

TABLE 4. Parameters of the alkaline electrolyzer and PEMFC.

Equipment	Rated power/W	Conversion efficiency
Alkaline electrolyzer	6000	80%
PEMFC	5000	50%

TABLE 5. Time of purchase and selling electricity price.

Type of time period	Time quantum	Purchase price of electricity/(CNY/kWh)	Price of electricity sold/(CNY/kWh)
Gentle	0:00-8:00	0.37	0.28
The second peak	8:00-12:00	0.87	0.72
	17:00-21:00	0.87	0.72
Peak	12:00-17:00	0.69	0.53
	21:00-24:00	0.69	0.53

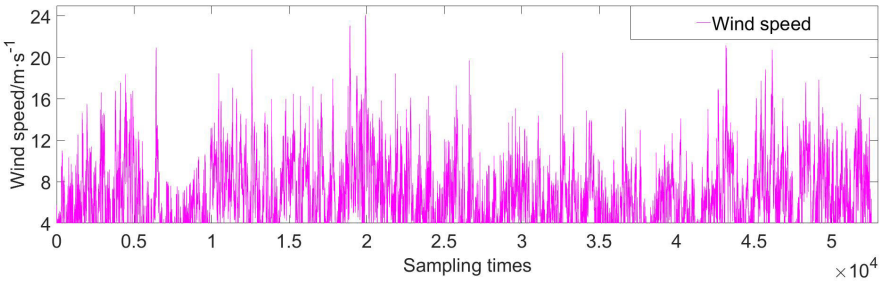

FIGURE 4. Local wind speed curve in 2019 (height of 10 m).

C. OPTIMIZATION RESULTS AND EXAMPLE CALCULATION AND ANALYSIS

To verify the effectiveness of the improved genetic algorithm (IGA) optimization, this paper uses the traditional genetic algorithm (GA), the traditional particle swarm optimization (PSO) and the nondominated sorting genetic algorithm (NSGA-II) to conduct an example comparison of the system optimization. The objective function is the maximum annual mean cost, and the system revenue mainly comes from hydrogen sales, oxygen sales and electricity sales. According to

TABLE 6. Improved genetic algorithm optimization results.

Optimization algorithm	The number of wind turbines	The number of photovoltaic panels	The number of lead-acid batteries	The number of alkaline electrolyzers	The number of PEMFCs	LPSP	ANC
IGA	3	23	82	1	1	0.00	144513
GA	2	42	193	1	1	0.00	171591
PSO	3	22	140	1	1	0.00	169227
NSGA-II	3	26	107	1	1	0.00	158421

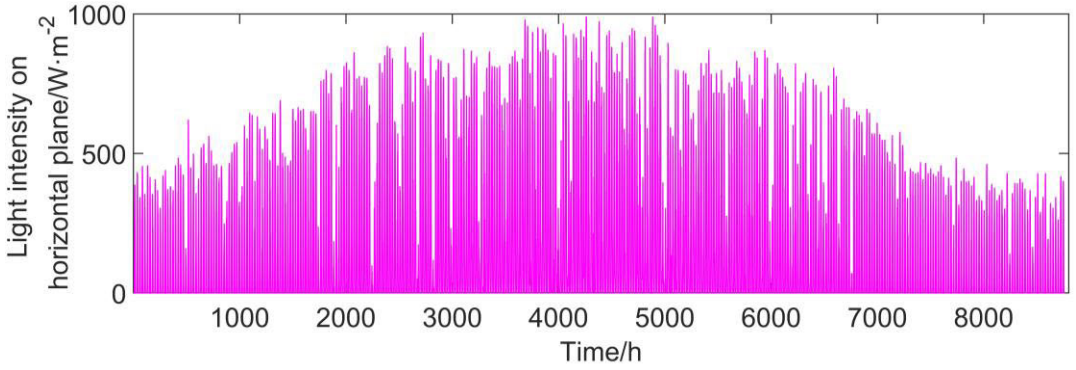

FIGURE 5. Local horizontal strength of the illumination curve in 2019.

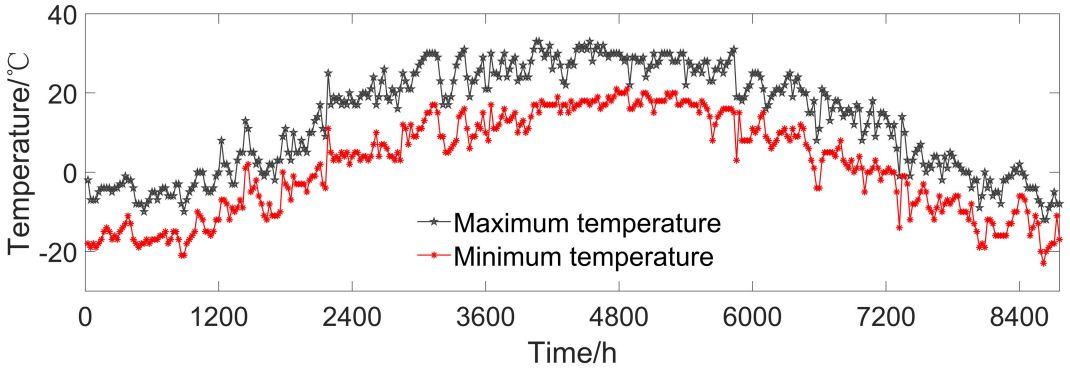

FIGURE 6. Maximum and minimum temperature of the environment.

local wind speed data, radiation intensity data and load data, the IGA is adopted for the optimization. The optimization results of the IGA, GA, PSO and NSGA-II are shown in TABLE 6.

As seen from TABLE 6, the optimization results of GA, PSO and NSGA-II are obviously inferior to those of IGA. The number of batteries in the three algorithms reached more than 100, which would greatly increase the construction costs and operation and maintenance costs of the system, and the replacement of equipment would be more complicated. In the optimization results, the GA optimization cost was 18.7% higher than the IGA optimization cost. The PSO optimization cost was 17.1% higher than the IGA optimization cost. The NSGA-II optimization cost was 9.6% higher than the IGA optimization cost. The comparison results showed that the IGA had the best optimization accuracy.

The iteration process curves of the three optimization algorithms are shown in FIGURE 8.

According to the iteration curves, the four optimization algorithms all fully converge within 120 iterations, but the GA convergence requires approximately 70 steps, the PSO convergence requires approximately 75 steps, the NSGA-II convergence requires approximately 58 steps. It is worth noting that the IGA convergence only needs approximately 45 steps. Therefore, through the comparison, IGA shows good adaptability to system optimization analyses with complex constraints and strong logic, such as a

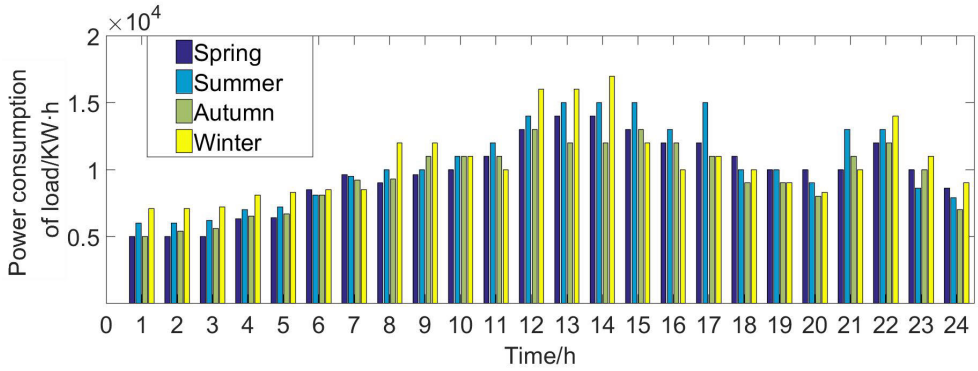

FIGURE 7. Annual local electricity loads in the study area.

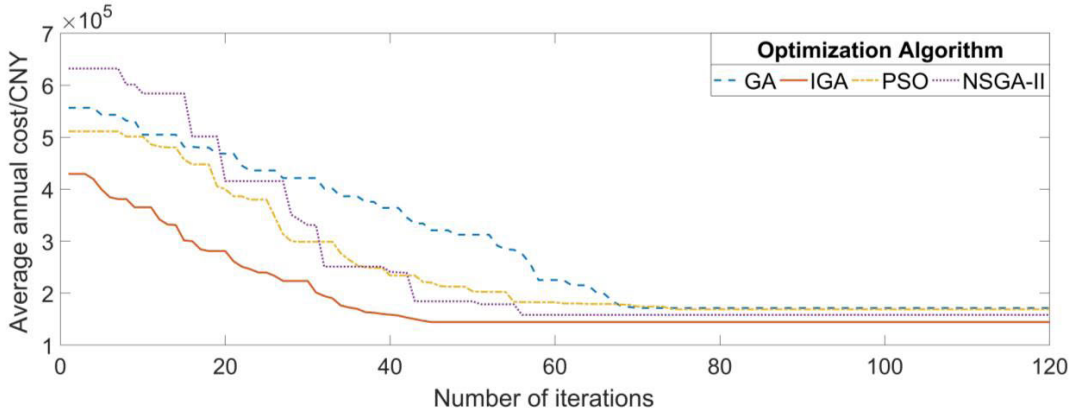

FIGURE 8. Iteration process curves of IGA, GA, PSO and NSGA-II.

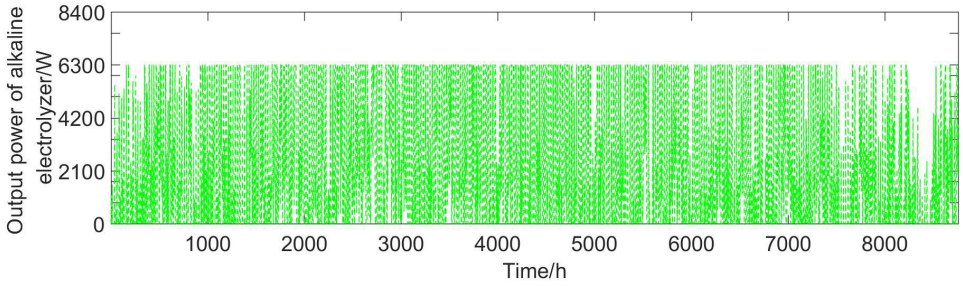

FIGURE 9. Output power curve of the electrolytic cell.

wind-solar-battery-fuel cell multienergy flow integrated power supply system optimization.

FIGURE 9 and FIGURE 10 show the output power curve of the electrolytic cell and the battery power curve, respectively. It can be seen from the two figures that the output power of the electrolytic cell is approximately 6300 W in 8760 hours a year, which meets the required safety conditions. The battery power state is maintained between 0.3-0.9, neither overcharged nor released, which is conducive to the safe and optimal operation of the battery. Other scholars have also mentioned similar conclusions.

The output power curves of the wind, solar and PEMFC components are shown in FIGURE 11.

It can be seen from FIGURE 11 that in 8760 hours of the whole year, wind power generation occupies the dominant position, followed by solar power generation, and the output of the fuel cell is the lowest. When wind and solar power generation cannot meet the load, the fuel cell output can supplement energy to meet the needs of users, and the solar power generation capacity is consistent with the irradiance data shown in FIGURE 5.

FIGURE 12 shows the annual quantities of electricity purchases and sold. It can be seen from the figure that the annual quantity of electricity sold will be greater than that purchased over the whole year. Therefore, it is of positive significance to establish a wind-solar-hydrogen storage and power supply system in this area.

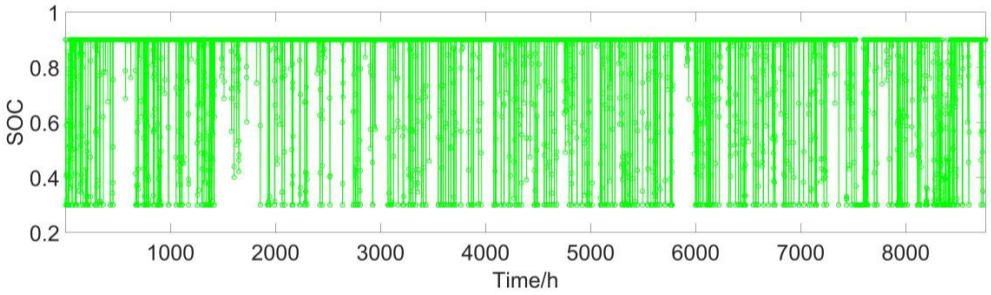

FIGURE 10. Curve of the SOC.

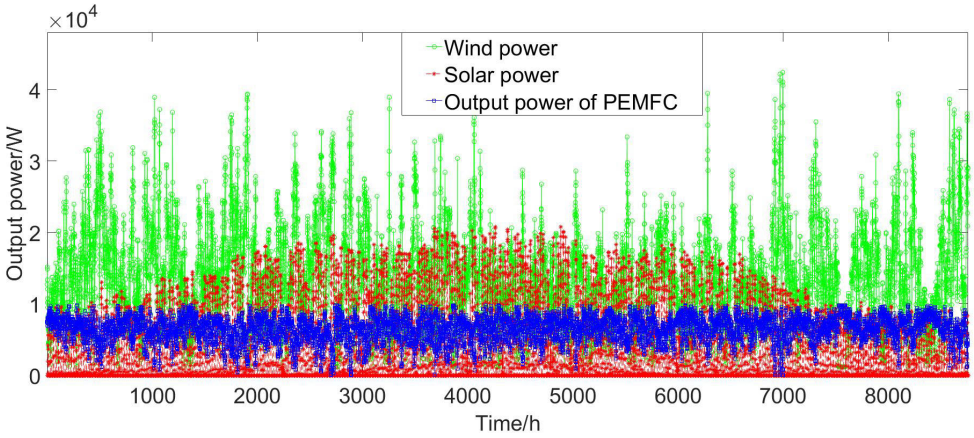

FIGURE 11. Output power curves of the wind turbine, photovoltaic panels and PEMFC.

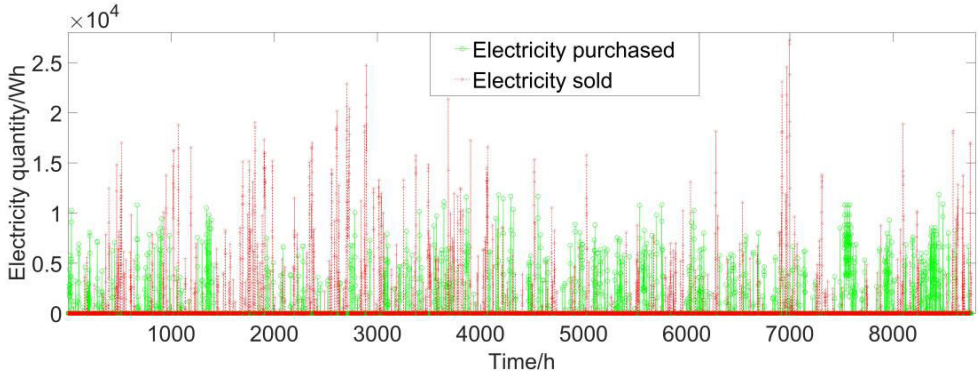

FIGURE 12. Purchase and sale of electricity.

VI. CONCLUSION

The object of this study is to optimize the grid-connected regional power supply, and to this end, a wind-solar-battery-fuel cell integrated power supply system is established. The system can electrolyze water with excess electricity while meeting the load's electricity demand. The excess electricity is converted into hydrogen. When the output electricity of the system cannot meet the load demand, hydrogen enters the PEMFC to continue the power supply. This system can fully meet the power demand for a given area and effectively reduce the local curtailment of wind energy and solar energy caused by poor power generation due to equipment capacity configurations.

An improved genetic algorithm is proposed to optimize the structure of the wind-solar-battery-fuel cell integrated power supply system, designed to supply a load with a known daily energy demand. An optimization model is established to take the annual average cost as the optimization goal and the battery power state and LPSP as the constraint conditions. In the optimization results, the IGA completely converged in approximately 45 steps. The cost calculation result of the GA was 18.7% higher than that of the IGA, and the GA completely converged at approximately 70 steps. The cost calculation result of the PSO was 17.1% higher than that of the IGA, and the PSO completely converged at approximately 75 steps. The cost calculation result of the NSGA-II was 9.6%

higher than that of the IGA, and the NSGA-II completely converged at approximately 58 steps. These results show that IGA not only has higher optimization accuracy, as reflected in the optimization results, but also uses the algorithm in less time, which verifies the good adaptability and effectiveness of the algorithm in strong logical multiobjective optimization problems.

However, the cost considered in this paper is too idealized; the costs of hydrogen transport, oxygen transport, system equipment installation labor, transmission loss, etc. were not considered, resulting in the a between the final cost and reality. This paper provides a reference basis for the future construction of a grid-connected wind-solar-hydrogen storage integrated power supply system aimed at regional power supply problems.

REFERENCES

[1] T. Li, Y. Song, and J. Shen, "Clean power dispatching of coal-fired power generation in China based on the production cleanliness evaluation method," *Sustainability*, vol. 11, no. 23, p. 6778, Nov. 2019.

[2] M. Liu, S. Wang, Y. Zhao, H. Tang, and J. Yan, "Heat–power decoupling technologies for coal-fired CHP plants: Operation flexibility and thermodynamic performance," *Energy*, vol. 188, Dec. 2019, Art. no. 116074.

[3] H. Wei, Z. Hongxuan, D. Yu, W. Yiting, D. Ling, and X. Ming, "Short-term optimal operation of hydro-wind-solar hybrid system with improved generative adversarial networks," *Appl. Energy*, vol. 250, pp. 389–403, Sep. 2019.

[4] K. Nusair and F. Alasali, "Optimal power flow management system for a power network with stochastic renewable energy resources using golden ratio optimization method," *Energies*, vol. 13, no. 14, p. 3671, Jul. 2020.

[5] H. Hou, T. Xu, X. Wu, H. Wang, A. Tang, and Y. Chen, "Optimal capacity configuration of the wind-photovoltaic-storage hybrid power system based on gravity energy storage system," *Appl. Energy*, vol. 271, Aug. 2020, Art. no. 115052.

[6] M. Khalid, M. AlMuhaini, R. P. Aguilera, and A. V. Savkin, "Method for planning a wind–solar–battery hybrid power plant with optimal generation-demand matching," *IET Renew. Power Gener.*, vol. 12, no. 15, pp. 1800–1806, Nov. 2018.

[7] J. Zhu, W. Yuan, M. Qiu, B. Wei, H. Zhang, P. Chen, Y. Yang, M. Zhang, X. Huang, and Z. Li, "Experimental demonstration and application planning of high temperature superconducting energy storage system for renewable power grids," *Appl. Energy*, vol. 137, pp. 692–698, Jan. 2015.

[8] N. Nabipour, S. N. Qasem, and K. Jermsittiparsert, "Type-3 fuzzy voltage management in PV/hydrogen fuel cell/battery hybrid systems," *Int. J. Hydrogen Energy*, vol. 45, no. 56, pp. 32478–32492, Nov. 2020.

[9] Z. Abdin and W. Mérida, "Hybrid energy systems for off-grid power supply and hydrogen production based on renewable energy: A techno-economic analysis," *Energy Convers. Manage.*, vol. 196, pp. 1068–1079, Sep. 2019.

[10] Z. Wu, P. F. Zhu, J. Yao, S. G. Zhang, J. W. Ren, F. S. Yang, and Z. X. Zhang, "Combined biomass gasification, SOFC, IC engine, and waste heat recovery system for power and heat generation: Energy, exergy, exergoeconomic, environmental (4E) evaluations," *Appl. Energy*, vol. 279, p. 19, Dec. 2020.

[11] P. Gabrielli, A. Poluzzi, G. J. Kramer, C. Spiers, M. Mazzotti, and M. Gazzani, "Seasonal energy storage for zero-emissions multi-energy systems via underground hydrogen storage," *Renew. Sustain. Energy Rev.*, vol. 121, Apr. 2020, Art. no. 109629.

[12] H. Mehrjerdi, "Peer-to-peer home energy management incorporating hydrogen storage system and solar generating units," *Renew. Energy*, vol. 156, pp. 183–192, Aug. 2020.

[13] H. Yang, Q. Li, S. Zhao, W. Chen, and H. Liu, "A hierarchical self-regulation control for economic operation of AC/DC hybrid microgrid with hydrogen energy storage system," *IEEE Access*, vol. 7, pp. 89330–89341, 2019.

[14] L. Valverde-Isorna, D. Ali, D. Hogg, and M. Abdel-Wahab, "Modelling the performance of wind–hydrogen energy systems: Case study the hydrogen office in Scotland/UK," *Renew. Sustain. Energy Rev.*, vol. 53, pp. 1313–1332, Jan. 2016.

[15] V. Kalkhambkar, R. Kumar, and R. Bhakar, "Joint optimal allocation methodology for renewable distributed generation and energy storage for economic benefits," *IET Renew. Power Gener.*, vol. 10, no. 9, pp. 1422–1430, Oct. 2016.

[16] V. Kalkhambkar, R. Kumar, and R. Bhakar, "Joint optimal sizing and placement of renewable distributed generation and energy storage for energy loss minimization," in *Proc. 4th Int. Conf. Adv. Comput. Commun. Syst. (ICACCS)*, Jan. 2017, pp. 1–9.

[17] J. Z. Li, P. Liu, and Z. Li, "Optimal design and techno-economic analysis of a solar-wind-biomass off-grid hybrid power system for remote rural electrification: A case study of West China," *Energy*, vol. 208, p. 12, Oct. 2020.

[18] L. Kasprzyk, A. Tomczewski, R. Pietracho, A. Mielcarek, Z. Nadolny, K. Tomczewski, G. Trzmiel, and J. Alemany, "Optimization of a solar-wind hybrid power supply structure with electrochemical storage intended for supplying a load with known characteristics," *Energies*, vol. 13, no. 22, p. 31, Nov. 2020.

[19] M. J. Mayer, A. Szilagyi, and G. Grof, "Environmental and eco-nomic multi-objective optimization of a household level hybrid renewable energy system by genetic algorithm," *Appl. Energy*, vol. 269, p. 16, Jul. 2020.

[20] M. S. Javed, A. Song, and T. Ma, "Techno-economic assessment of a stand-alone hybrid solar-wind-battery system for a remote island using genetic algorithm," *Energy*, vol. 176, pp. 704–717, Jun. 2019.

[21] S. Guo, Y. He, H. Pei, and S. Wu, "The multi-objective capacity optimization of wind-photovoltaic-thermal energy storage hybrid power system with electric heater," *Sol. Energy*, vol. 195, pp. 138–149, Jan. 2020.

[22] A. Fetanat and E. Khorasaninejad, "Size optimization for hybrid photovoltaic–wind energy system using ant colony optimization for continuous domains based integer programming," *Appl. Soft Comput.*, vol. 31, pp. 196–209, Jun. 2015.

[23] E. Dilettoso and N. Salerno, "A self-adaptive niching genetic algorithm for multimodal optimization of electromagnetic devices," *IEEE Trans. Magn.*, vol. 42, no. 4, pp. 1203–1206, Apr. 2006.

[24] S.-F. Hwang and R.-S. He, "Improving real-parameter genetic algorithm with simulated annealing for engineering problems," *Adv. Eng. Softw.*, vol. 37, no. 6, pp. 406–418, Jun. 2006.

[25] A. A. Mohamed, S. Ali, S. Alkhalaf, T. Senjyu, and A. M. Hemeida, "Optimal allocation of hybrid renewable energy system by multi-objective water cycle algorithm," *Sustainability*, vol. 11, no. 23, p. 20, Dec. 2019.

[26] W. Q. Dong, Y. J. Li, and J. Xiang, "Sizing of a stand-alone photovoltaic/wind energy system with hydrogen and battery storage based on improved ant colony algorithm," in *Proc. 28th Chin. Control Decis. Conf.*, May 2016, pp. 4461–4466.

[27] D. B. Zhang, J. W. Liu, S. F. Jiao, H. Tian, C. Z. Lou, Z. H. Zhou, J. Zhang, C. D. Wang, and J. Zuo, "Research on the configuration and operation effect of the hybrid solar-wind-battery power generation system based on NSGA-II," *Energy*, vol. 189, p. 11, Dec. 2019.

[28] C. B. Xu, Y. M. Ke, Y. B. Li, H. Chu, and Y. N. Wu, "Data-driven configuration optimization of an off-grid wind/SOLAR/hydrogen system based on modified NSGA-II and CRITIC-TOPSIS," *Energy Convers. Manage.*, vol. 215, p. 18, Jul. 2020.

[29] M. Jahangiri, M. H. Soulouknga, F. K. Bardei, A. A. Shamsabadi, E. T. Akinlabi, S. M. Sichilalu, and A. Mostafaeipour, "Techno-econo-environmental optimal operation of grid-wind-solar electricity generation with hydrogen storage system for domestic scale, case study in chad," *Int. J. Hydrogen Energy*, vol. 44, no. 54, pp. 28613–28628, Nov. 2019.

[30] Z. Hao, W. Qiuxuan, C. Xiaoni, L. Weijie, and L. Yanbin, "Research on optimization scheduling of wind/solar/diesel/storage micro-grid based on genetic algorithm," in *Proc. 36th Chin. Control Conf. (CCC)*, T. Liu and Q. Zhao, Eds. New York, NY, USA, Jul. 2017, pp. 9341–9348.

[31] M. Ding, Y. Zhang, M. Mao, W. Yang, and X. Liu, "Steady model and operation optimization for microgrids under centralized control," *Dianli Xitong Zidonghua/Automat. Electr. Power Syst.*, vol. 33, no. 24, pp. 78–82, 2009.

[32] R. Belfkira, O. Hajji, C. Nichita, and G. Barakat, "Optimal sizing of stand-alone hybrid wind/SOLAR system with battery storage," in *Proc. Eur. Conf. Power Electron. Appl.* Piscataway, NJ, USA: IEEE, Sep. 2007, pp. 4339–4348.

[33] Y. Devrim and L. Bilir, "Performance investigation of a wind turbine–solar photovoltaic panels–fuel cell hybrid system installed at Incek region–Ankara, Turkey," *Energy Convers. Manage.*, vol. 126, pp. 759–766, Oct. 2016.

[34] O. Ulleberg, "Modeling of advanced alkaline electrolyzers: A system simulation approach," *Int. J. Hydrogen Energy*, vol. 28, no. 1, pp. 21–33, Jan. 2003.
[35] Y.-F. Guo, H.-C. Chen, and F.-C. Wang, "The development of a hybrid PEMFC power system," *Int. J. Hydrogen Energy*, vol. 40, no. 13, pp. 4630–4640, Apr. 2015.
[36] C. Gnanavel and S. A. Alexander, "Experimental validation of an eleven level symmetrical inverter using genetic algorithm and queen bee assisted genetic algorithm for solar photovoltaic applications," *J. Circuits, Syst. Comput.*, vol. 27, no. 13, Dec. 2018, Art. no. 1850212.
[37] H. Shi, L. Li, and C. Zhao, "Optimization of wind-marine hybrid power system configuration based on genetic algorithm," *J. Ocean Univ. China*, vol. 16, no. 4, pp. 709–715, Aug. 2017.
[38] M. Burakov and V. Shishlakov, "Genetic algorithm optimization for pitch angle control of variable speed wind turbines," in *Proc. 12th Int. Sci.-Tech. Conf. Electromechanics Robot. Zavalishins Readings (ER (ZR), MATEC Web Conf.*, A. Ronzhin and V. Shishlakov, Eds. St Petersburg, Russia: EDP Sciences, Apr. 2017, Art. no. 01009.
[39] A. Mahesh and K. S. Sandhu, "A genetic algorithm based improved optimal sizing strategy for solar-wind-battery hybrid system using energy filter algorithm," *Frontiers Energy*, vol. 14, no. 1, pp. 139–151, Mar. 2020.
[40] D. Vallejo, E. Cornalino, and R. Chaer, "Genetic algorithm applied to the specialization of neural networks for the forecast of wind and solar generation," in *Proc. 9th IEEE Power, Instrum. Meas. Meeting (EPIM)*, New York, NY, USA, Nov. 2018.
[41] T. Sarkar, A. Bhattacharjee, H. Samanta, K. Bhattacharya, and H. Saha, "Optimal design and implementation of solar PV-wind-biogas-VRFB storage integrated smart hybrid microgrid for ensuring zero loss of power supply probability," *Energy Convers. Manage.*, vol. 191, pp. 102–118, Jul. 2019.
[42] A. Maleki and A. Askarzadeh, "Artificial bee swarm optimization for optimum sizing of a stand-alone SOLAR/WT/FC hybrid system considering LPSP concept," *Sol. Energy*, vol. 107, pp. 227–235, Sep. 2014.
[43] A. Maleki and F. Pourfayaz, "Optimal sizing of autonomous hybrid photovoltaic/wind/battery power system with LPSP technology by using evolutionary algorithms," *Sol. Energy*, vol. 115, pp. 471–483, May 2015.
[44] H. Yang, W. Zhou, L. Lu, and Z. Fang, "Optimal sizing method for stand-alone hybrid solar–wind system with LPSP technology by using genetic algorithm," *Sol. Energy*, vol. 82, no. 4, pp. 354–367, Apr. 2008.
[45] H. Yang, Z. Gong, Y. Ma, L. Wang, and B. Dong, "Optimal two-stage dispatch method of household PV-BESS integrated generation system under time-of-use electricity price," *Int. J. Electr. Power Energy Syst.*, vol. 123, Dec. 2020, Art. no. 106244.

ZEKUN WANG was born in Chifeng, Inner Mongolia, China, in 1998. He received the B.E. degree in energy and power engineering from the Inner Mongolia University of Technology, in 2019, where he is currently pursuing the M.A.Eng. degree.

YAN JIA received the B.E. and M.A.Eng. degrees in energy and power engineering from the Inner Mongolia University of Technology, in 1996 and 2001, respectively, and the Ph.D. degree in engineering from Mie University, Japan, in 2008. She was an SVBL Foreign Researcher with the Graduate School of Engineering, Mie University, from 2008 to 2009. She is currently a Professor with the School of Energy and Power Engineering, Inner Mongolia University of Technology. Her main research interests include the development and utilization of new energy, composite energy storage and its control, and off-grid wind and solar hybrid power generation systems.

CHANG CAI received the Ph.D. degree from the Department of Energy and Power Engineering, Tsinghua University, in 2018. After graduation, he joined the Institute of Engineering Thermophysics, Chinese Academy of Sciences, as an Assistant Professor. His major research interests include wind energy, wind turbine aerodynamics, flow control, and computational fluid dynamics.

YINPENG CHEN received the B.E. degree in energy and power engineering from the University of South China, in 2019. He is currently pursuing the M.A.Eng. degree with the Inner Mongolia University of Technology.

NA LI received the B.E. degree in electrical engineering and automation from the College of Modern Science and Technology, Hebei Agricultural University, in 2018. She is currently pursuing the M.A.Eng. degree with the Inner Mongolia University of Technology.

MIAO YANG received the B.E. degree in building environment and energy application engineering from Shandong Agricultural University, in 2017. He is currently pursuing the M.A.Eng. degree with the Inner Mongolia University of Technology.

QING'AN LI received the B.E. degree from Naval Aviation University, in 2009, the M.A.Eng. degree from the Inner Mongolia University of Technology, in 2012, and the Ph.D. degree from Mie University, Japan, in 2015. From 2015 to 2018, he was a Researcher with Mie University. In 2018, he was with the Japanese Society for the Promotion of Science (JSPS) Talent Program, mainly engaged in wind energy utilization research. In 2018, he also joined the Institute of Engineering Thermophysics, Chinese Academy of Sciences, as a Researcher.